eLIFE
elifesciences.org

Figures and figure supplements

Allosteric inhibition of a stem cell RNA-binding protein by an intermediary metabolite

Carina C Clingman, et al.

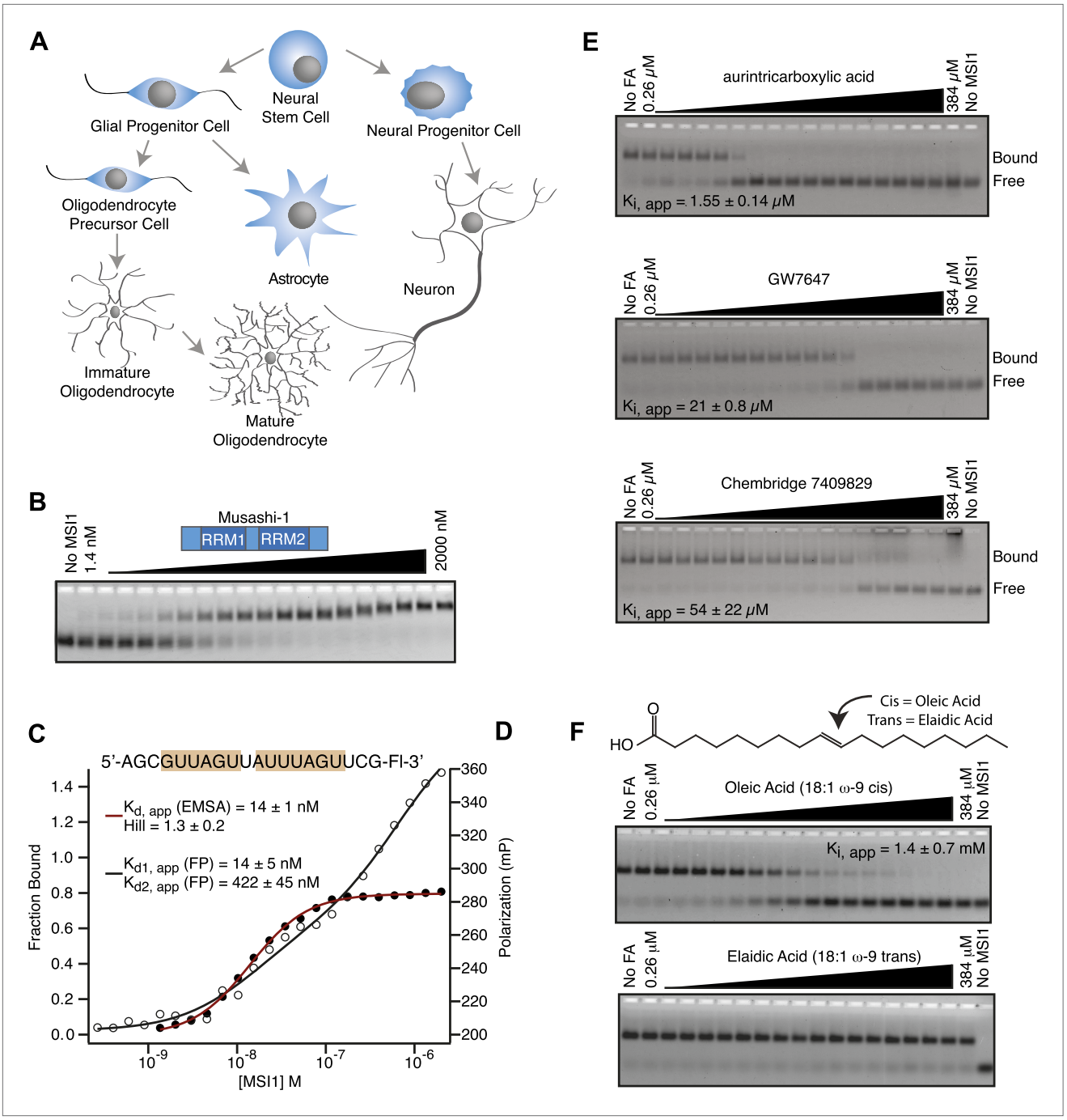

Figure 1. MSI1 is inhibited by monounsaturated fatty acids. (**A**) Pattern of MSI1 (blue) in the CNS. (**B**–**D**) EMSA and FP of MSI1 binding to RNA aptamer CCCR005 (AGCGUUAGUUAUUUAGUUCG). EMSA data (red line) were fit to the Hill equation where all shifted species were fit as an aggregate. FP data (black line) were fit to a two-site binding model. (**E** and **F**) Assay scheme for the inhibitor screen (**E**) and F–EMSA dose responses with hits identified from the small molecule screens (**E**) and oleic and elaidic acid (**F**). Each gel is one representative experiment of at least three independent experiments. No compound and no protein lanes identify the position of bound and free RNA migration, respectively.

DOI: 10.7554/eLife.02848.003

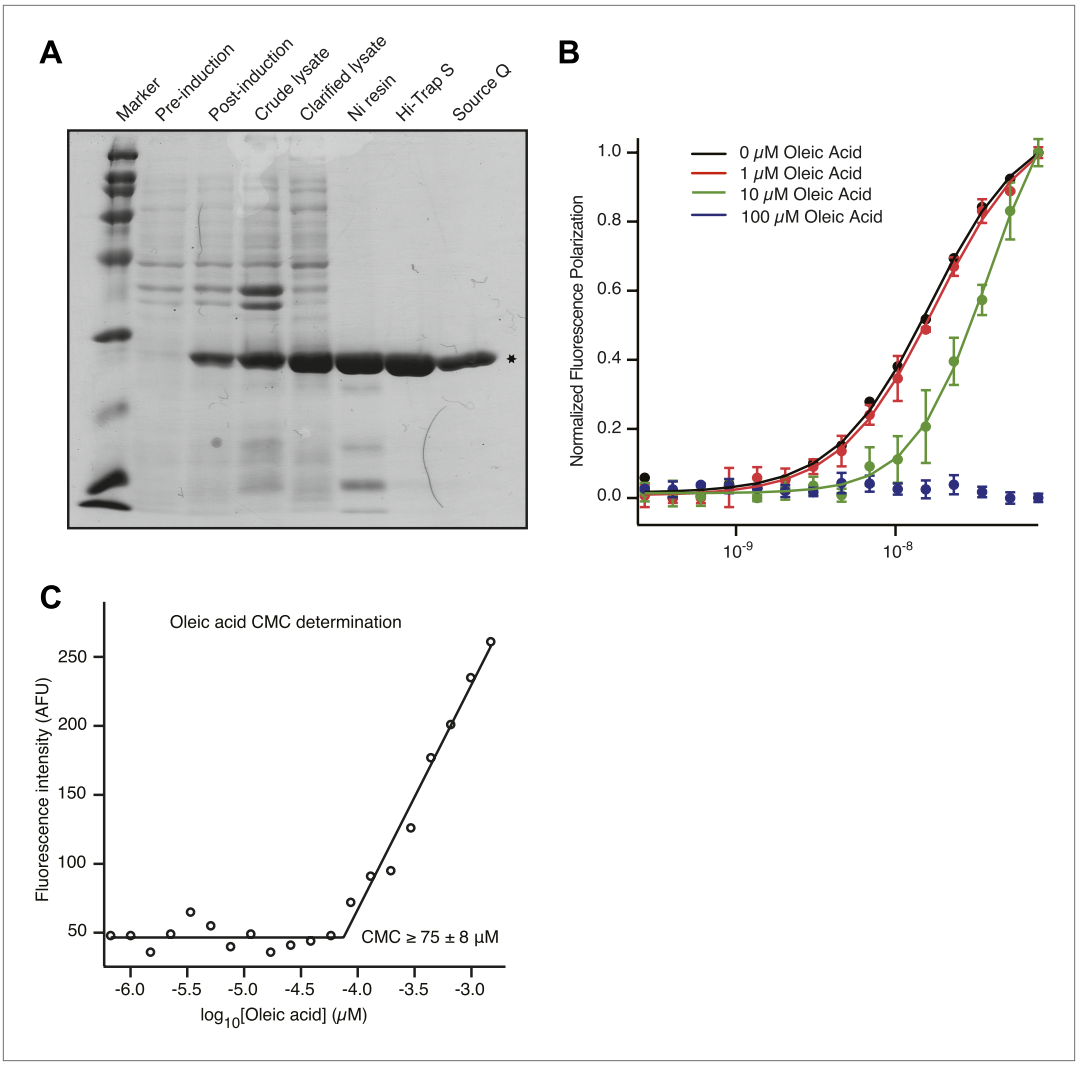

Figure 1—figure supplement 1.

DOI: 10.7554/eLife.02848.004

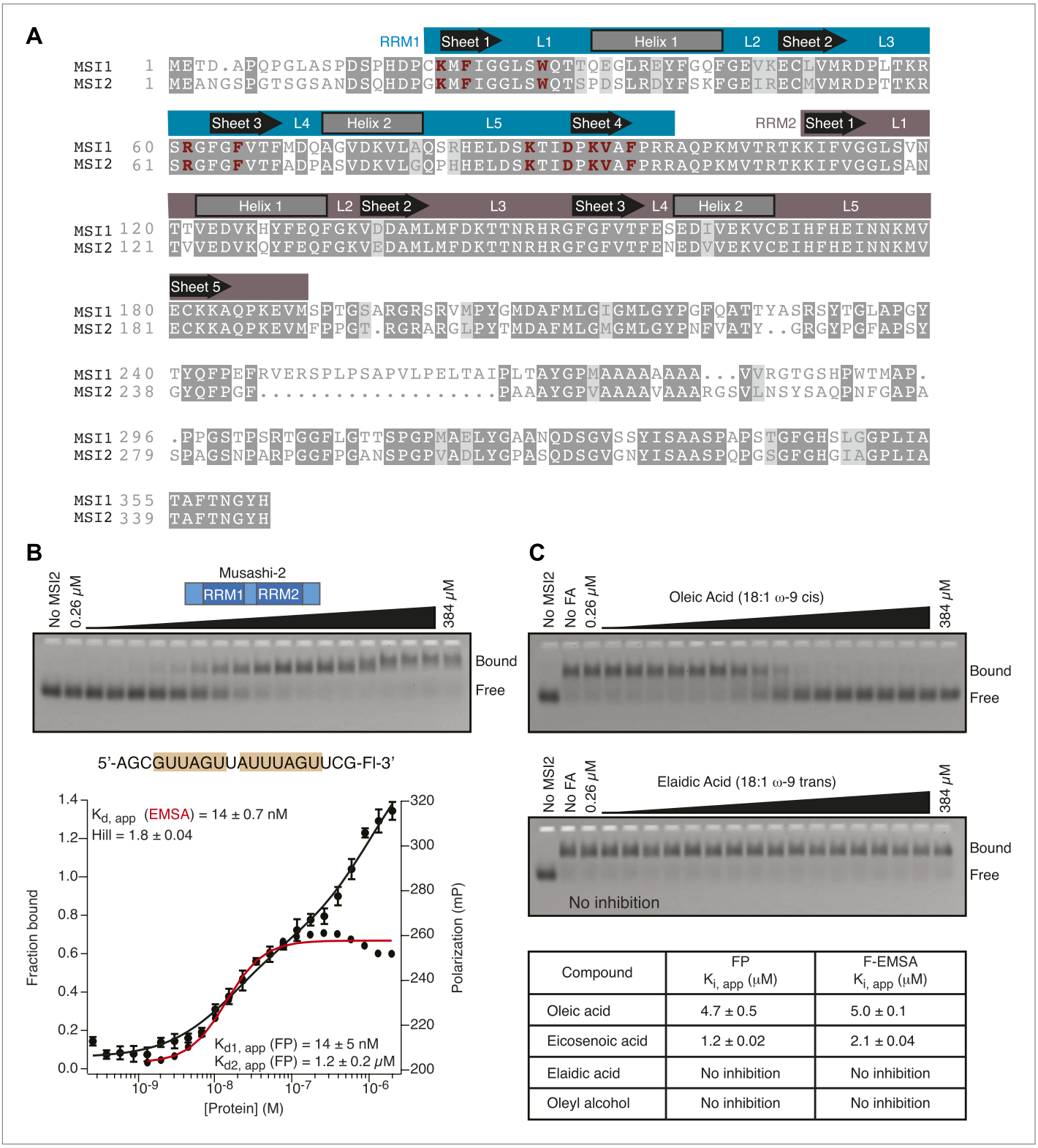

Compound	FP $K_{i, app}$ (μM)	F-EMSA $K_{i, app}$ (μM)
Oleic acid	4.7 ± 0.5	5.0 ± 0.1
Eicosenoic acid	1.2 ± 0.02	2.1 ± 0.04
Elaidic acid	No inhibition	No inhibition
Oleyl alcohol	No inhibition	No inhibition

Figure 1—figure supplement 2. RNA binding specificity and inhibition by specific fatty acids is conserved in MSI2.

DOI: 10.7554/eLife.02848.005

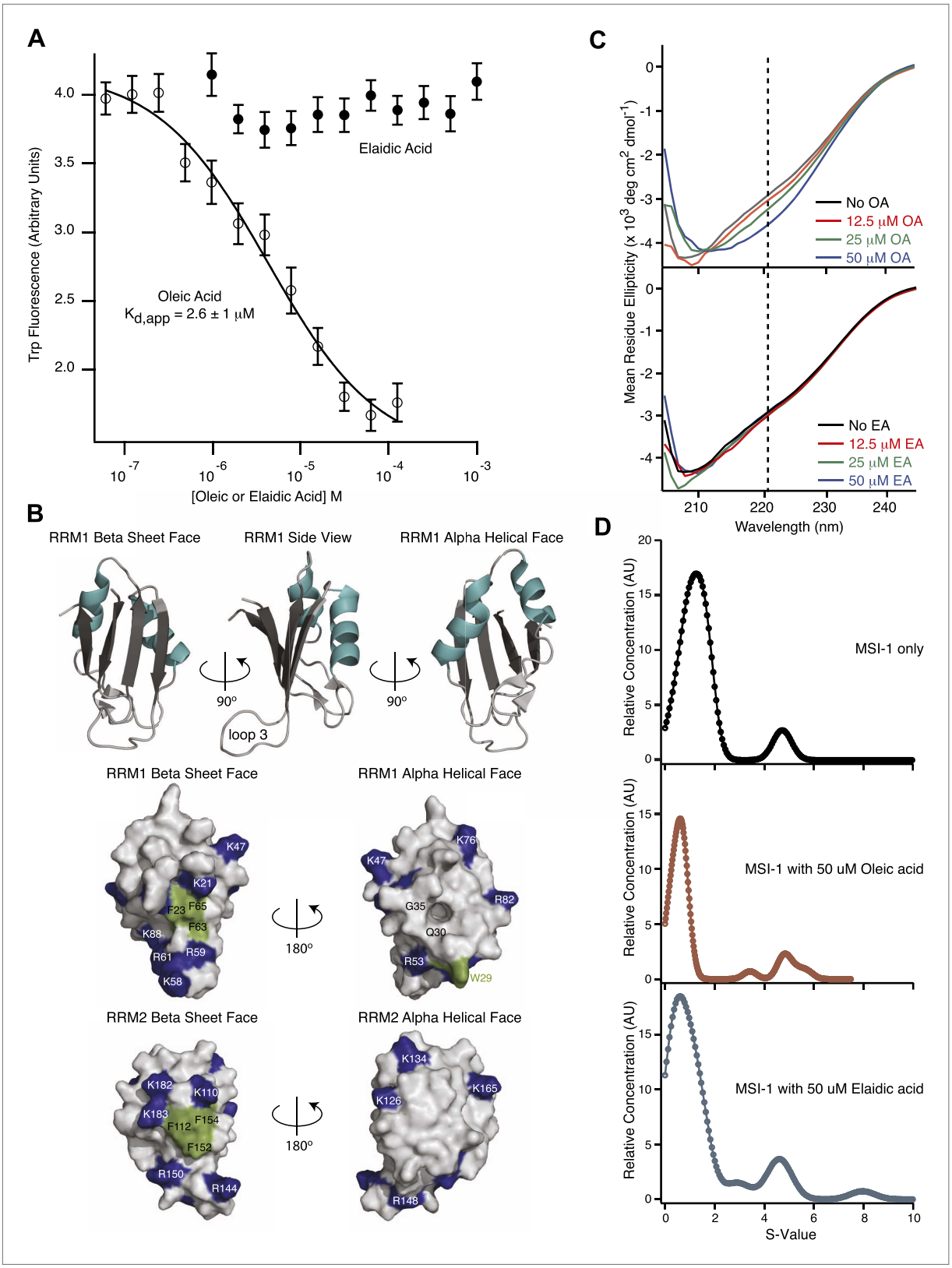

Figure 2. MSI1 inhibition is allosteric. (**A**) MSI1 tryptophan fluorescence at 350 nm as a function of oleic and elaidic acid. The $K_{d,\,app}$, $K_{i,\,app}$, and Hill parameters are the average and standard deviation of three independent replicates. (**B**) Ribbon model of MSI1 RRM1 (top). Space-filling model of MSI1 RRM1 (middle) and RRM2 (bottom) (***Nagata et al., 1999***; ***Miyanoiri et al., 2003***). Left, β-sheet surface, right, α-helical surface. Conserved phenylalanines

Figure 2. Continued on next page

Figure 2. Continued

and W29 are green. Lysine and arginine residues are blue. A hydrophobic pocket exists on the RRM1 α-helical surface. (**C**) CD spectra of MSI1 RRM1 in the presence of oleic (top) or elaidic acid (bottom). (**D**) Envelope traces of the van Holde-Weischet analysis for analytical ultracentrifugation experiments of MSI1 alone (top), with oleic acid (middle) and with elaidic acid (bottom). The predominant species sediments where monomeric MSI1 would be expected, and there is no significant change in the sedimentation profile after addition of oleic or elaidic acid. Data are representative traces from one of three independent experiments.

DOI: 10.7554/eLife.02848.007

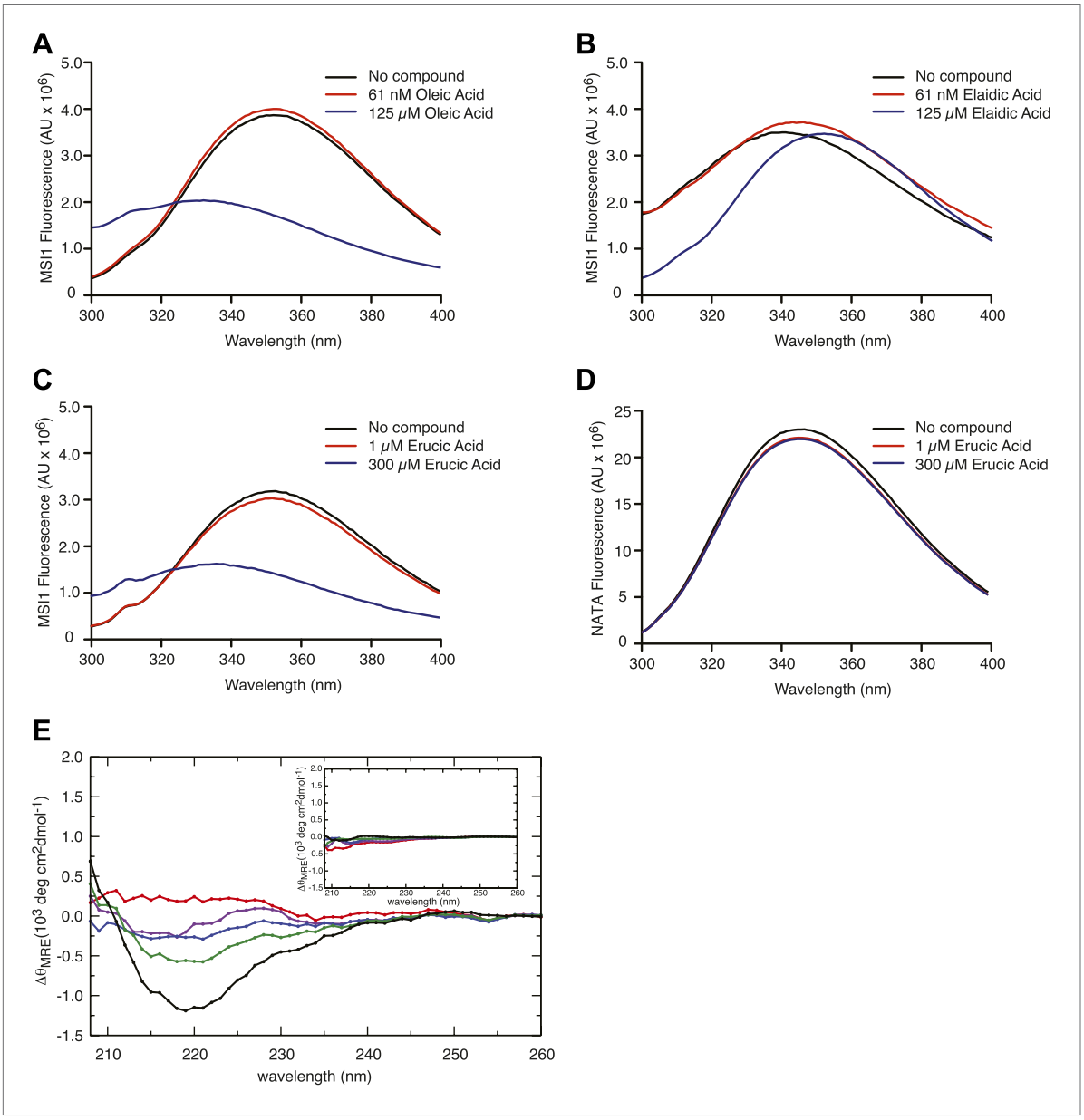

Figure 2—figure supplement 1.

DOI: 10.7554/eLife.02848.008

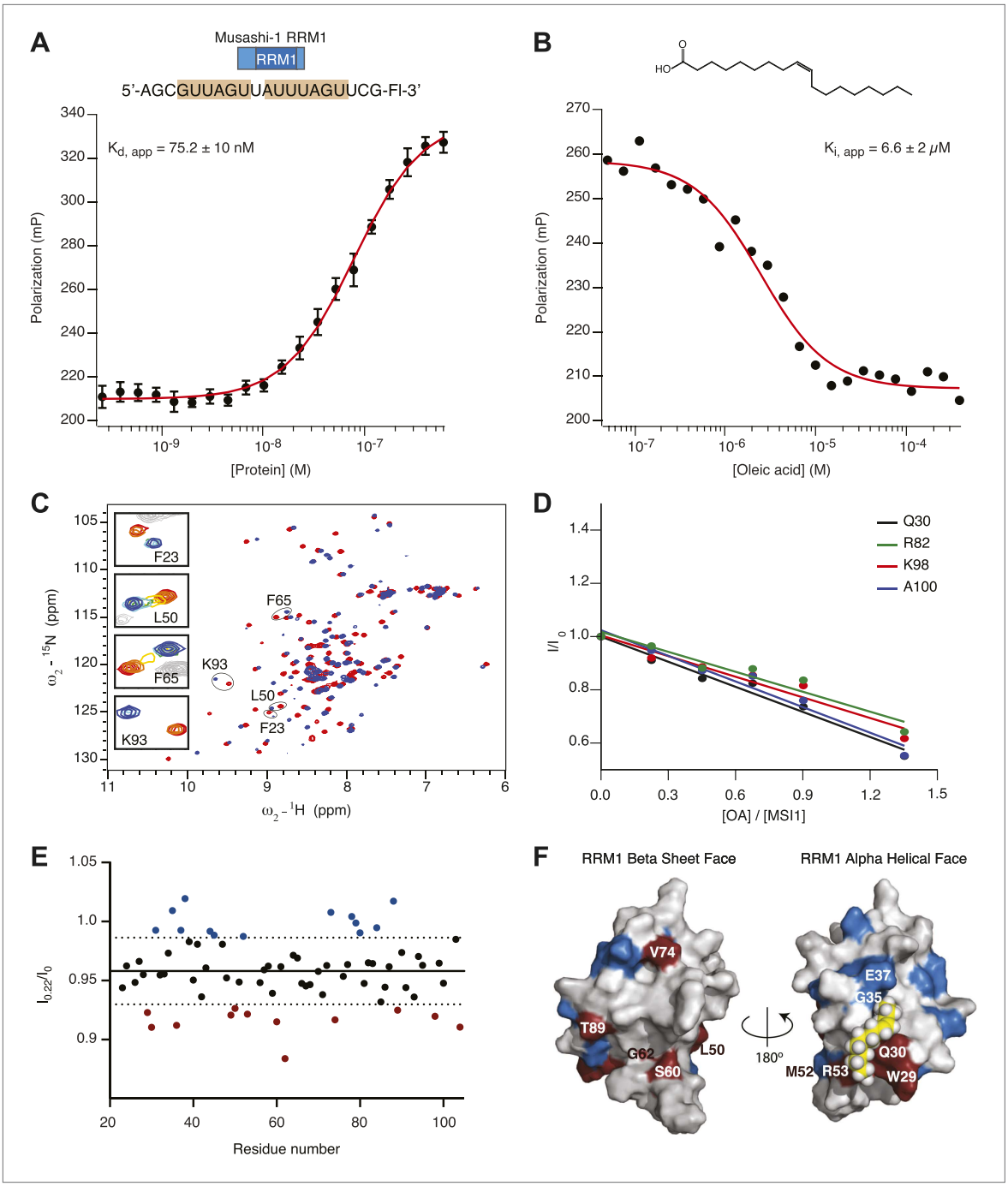

Figure 2—figure supplement 2.

DOI: 10.7554/eLife.02848.009

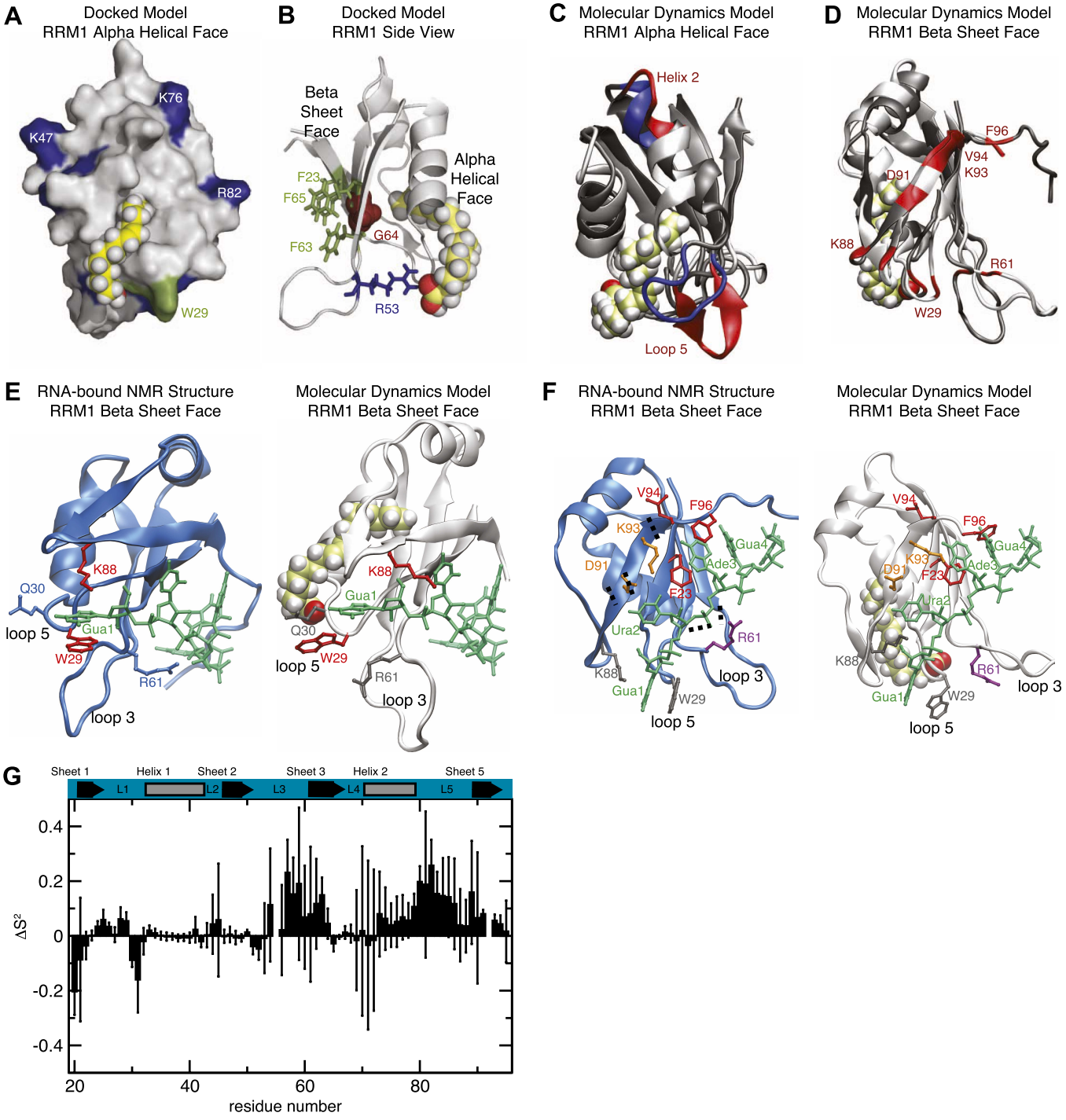

Figure 3. (**A** and **B**) Model of RRM1 bound to oleic acid (yellow) calculated by Schrödinger GLIDE (***Friesner et al., 2004***; ***Friesner et al., 2006***). (**C**) Overlay of the oleic acid bound MD simulation (gray and red) with the apo-state NMR structure (gray and blue) (***Ohyama et al., 2011***). (**D**) RNA contact residues (red) in loop 5, helix 2, and strand 4 of the β-sheet are perturbed in oleic acid-bound molecular dynamics simulation (***Ohyama et al., 2011***). (**E** and **F**) A representative snapshot from the MD simulation of MSI1 bound to oleic acid (white) compared to the MSI1-RNA NMR structure (blue) (***Ohyama et al., 2011***). Panel (**E**) shows the Gua 1 binding pocket. In the oleic-bound state, the open conformation of loop 5 (L5) orients K88 such that K88 cannot contact Gua 1. W29 is stacked against Q30 and unavailable for stacking against Gua 1. Interaction with the side chain of R61 stabilizes the conformation of W29 in the oleic-bound state. Panel (**F**) highlights the different conformations of residues that interact with Gua 1, Ura 2, Ade 3, and Gua 4; represented in grey, orange, red, and purple, respectively. (**G**) Difference of the mean Lipari-Szabo order parameters by residue between the apo and

Figure 3. Continued on next page

Figure 3. Continued

oleic acid-bound states of MSI1. The Lipari-Szabo order parameters for the backbone NH bond vectors, S^2, were calculated to quantify the backbone flexibility of the free and oleic acid-bound form of MSI1. The difference of the order parameters, $\Delta S^2 = S^2_{apo} - S^2_{MSI-OA}$, indicates that MSI1-oleic acid complex is more flexible than apo MSI1, with the few exceptions mostly observed at the N-terminus. The secondary structural elements are highlighted at the top. Error bars are calculated from the standard deviation among trajectories.

DOI: 10.7554/eLife.02848.010

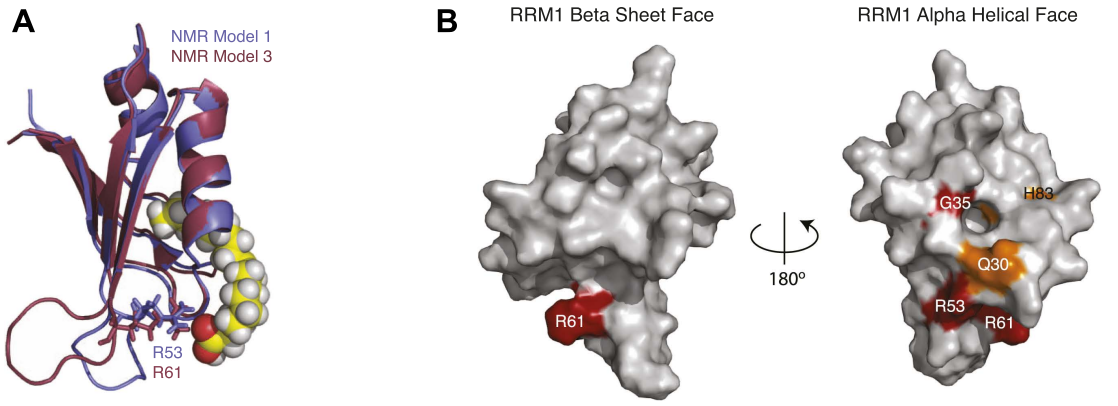

C

Protein	RNA binding affinity 5'-AGCGUUAGUUAUUUAGUUCG-Fl-3'		RNA binding inhibition by oleic acid	
	$K_{d,app}$ (nM)	Relative affinity	$K_{i,app}$ (μM)	Relative inhibition
WT	3.0 ± 2	1.0	0.48 ± 0.01	1.0
Q30E	2.3 ± 0.6	0.8	0.45 ± 0.03	0.9
G35D	7.1 ± 0.4	2.4	0.90 ± 0.08	1.9
G35E	30 ± 3	10.2	3.4 ± 1	7.1
H83F	7.7 ± 0.9	2.6	0.89 ± 0.1	1.9
H83L	6.5 ± 0.1	2.2	0.64 ± 0.02	1.3
G64A	27 ± 2	9.0	1.5 ± 0.4	3.1
R53E	9.0 ± 0.9	3.0	1.4 ± 0.1	3.0
R61E	53 ± 8	17.8	2.4 ± 0.3	5.0
R53E/R61E	97 ± 10	32.7	17 ± 3	34.9
R53E/R59E/R61E	146 ± 10	49.11	13 ± 5	27.0

Figure 3—figure supplement 1. Mutational analysis supports molecular dynamics simulation and docked model predictions.

DOI: 10.7554/eLife.02848.011

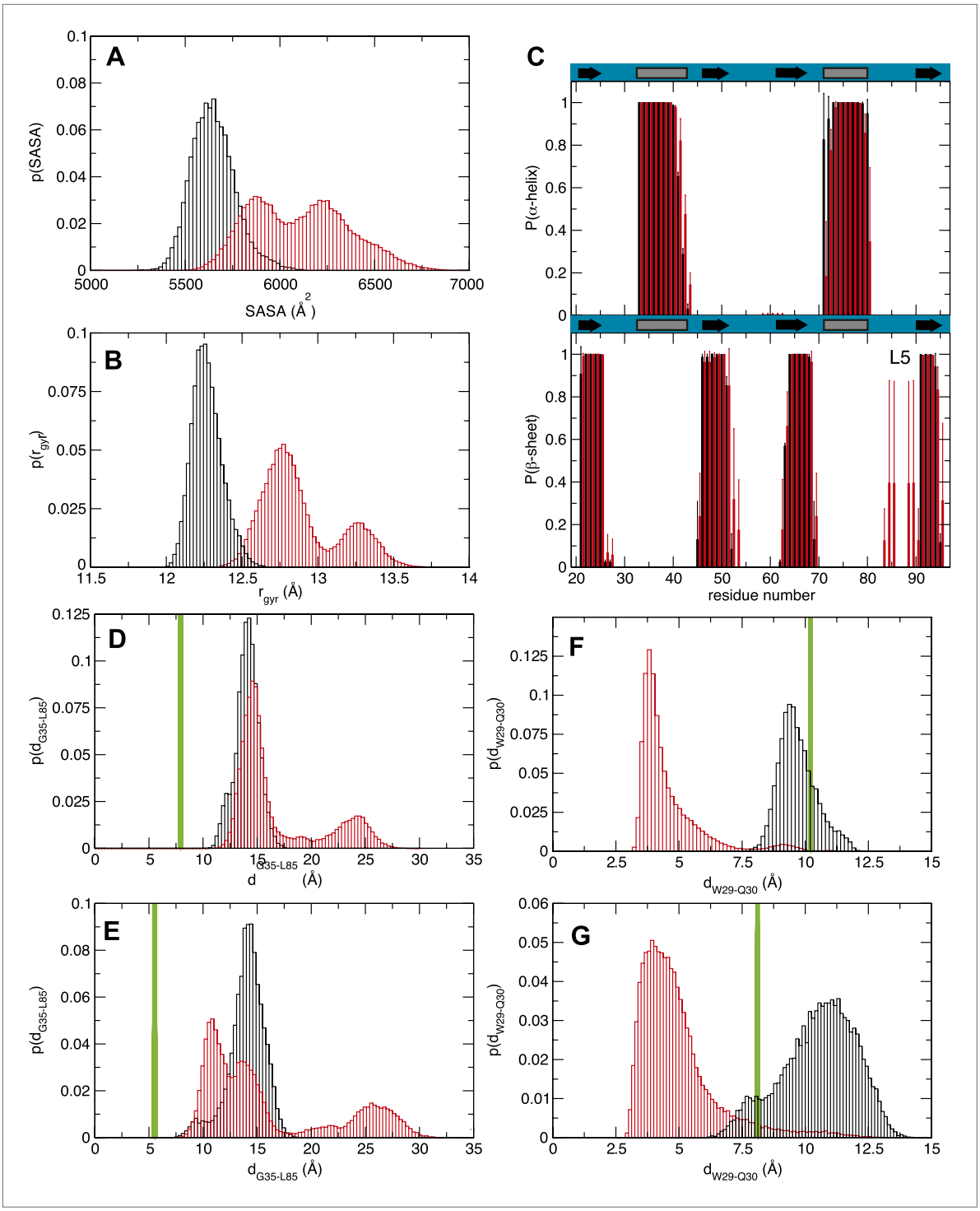

Figure 4. Molecular dynamics studies (**A** and **B**) represent the normalized histograms of the protein solvent accessible surface area (SASA) and radius of gyration (r_{gyr}) illustrating the structural transition undergone by the MSI1 upon oleic acid binding. (**A**) SASA distributions calculated from the MD trajectories of MSI1 bound to oleic acid and of MSI1 in the apo state are represented in red and black, respectively. (**B**) Radius of gyration distributions calculated from the MD trajectories of MSI-1 bound to oleic acid and of MSI1 in the apo state are represented in red and black, respectively. (**C**) The probability of being in an α-helix or β-sheet is shown for each residue of MSI1. The probabilities calculated for each residue from the MD trajectories of MSI1 free and bound to oleic acid are shown in black and red, respectively. Oleic acid binding is associated with stabilization of the C-terminus of α-helix 1, fraying of α-helix 2, at both the N- and C-termini, extension of sheet 2, as well as the formation of an additional β-sheet at loop 5 (L5). (**D** and **E**) Normalized histograms of the distance between G35, located on α-helix 1, and L85, located on loop 5, calculated from the MD trajectories of oleic acid-bound MSI-1

Figure 4. Continued on next page

Figure 4. Continued

and of apo MSI1 are shown in red and black, respectively. The distribution of distances between the C_α atoms of G35 and L85 is depicted in (**D**). The distribution of distances between the C_α of G35 and the $C_{\delta 2}$ of L85 is shown in (**E**). The green lines show the values of these distances observed in the NMR structure of MSI1 bound to RNA (PDB ID 2RS2). In the oleic-bound state, loop 5 is restricted in approaching α-helix 1 due to the steric hindrance of the oleic acid. (**F** and **G**) Normalized histograms of two representative side chain distances of W29 and Q30. Histograms calculated over the MD trajectories of oleic acid-bound MSI1 are shown in red, those of apo MSI1 in black. The distance between W29 $C_{\varepsilon 2}$ and Q30 C_γ is shown in (**F**). The distance between W29 $C_{\zeta 2}$ and Q30 $N_{\varepsilon 2}$ is shown in (**G**). The green lines show these distances observed in the NMR structure of MSI1 bound to RNA (PDB ID 2RS2). In the oleic-bound state, the side chain of W29 is stacked against the side chain of Q30. This conformation of W29 is not observed in either the free or RNA-bound states of MSI1.

DOI: 10.7554/eLife.02848.012

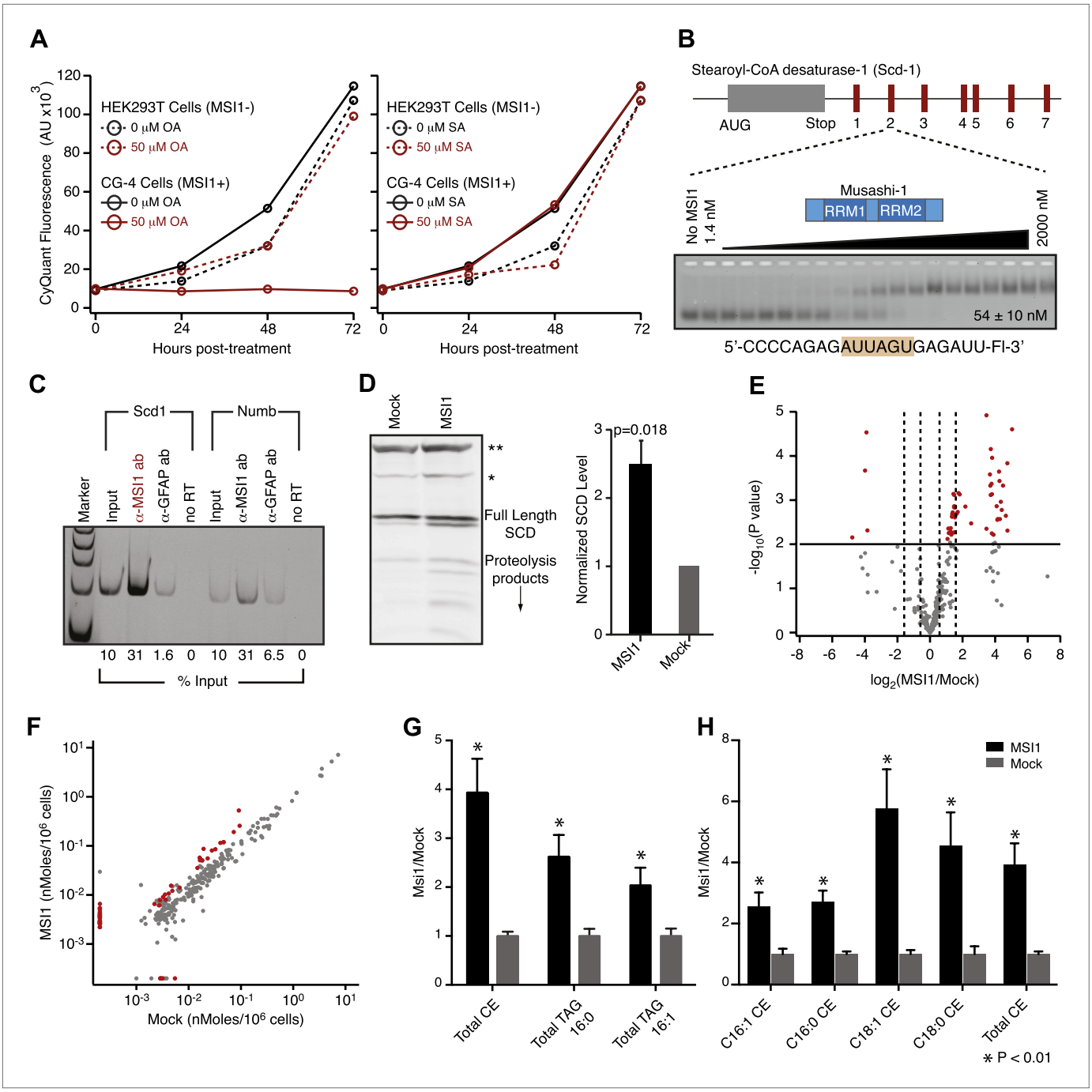

Figure 5. MSI-1 regulates stearoyl-CoA desaturase. (**A**) HEK293T (dashed) and CG-4 (solid) cell proliferation as a function of oleic acid or stearic acid treatment (red = treated, black = untreated). The data are the average and standard deviation of at least three biological replicates. (**B**) There are seven MSI1 consensus sites in the 3′-UTR of *Scd-1* mRNA. The $K_{d,\ app}$ is the average and standard deviation of at least three experiments. (**C**) *Scd-1* transcripts co-immunoprecipitate with anti-MSI1 antibodies. The data were quantified using a FUJI FLA-5000 imager. (**D**) Western analysis of SCD expression in HEK293T cells. The data were quantified using the LICOR Odyssey system relative to non specific bands (** and *, ***Figure 5—figure supplement 2B***) to control for loading. The average and standard deviation of at least three independent experiments is shown. (**E**–**H**) Lipidomics analysis of HEK293T cells ± MSI1 expression. Source data are included in ***Figure 5—source data 1***. (**E**) Volcano plot of lipidomics data. Dashed lines denote fold-changes of ±1.5 and ±3. Red data points indicate lipids that are significantly changed upon MSI1 expression. (**F**) Scatter plot of lipidomics data. Data are reported as nMoles per million cells. Red data points indicate lipids that are significantly changed upon MSI1 expression (FDR = 0.05). (**G**) Fold-changes of the total cholesterol esters and two TAG classes in which 38 of the 54 significantly changing lipids are categorized. Each class changes significantly with MSI1 overexpression ($p<0.05$). (**H**) Fold-changes for the four lipids that comprise the total cholesterol esters class. All display significant changes with MSI1 expression (FDR = 0.05).

DOI: 10.7554/eLife.02848.014

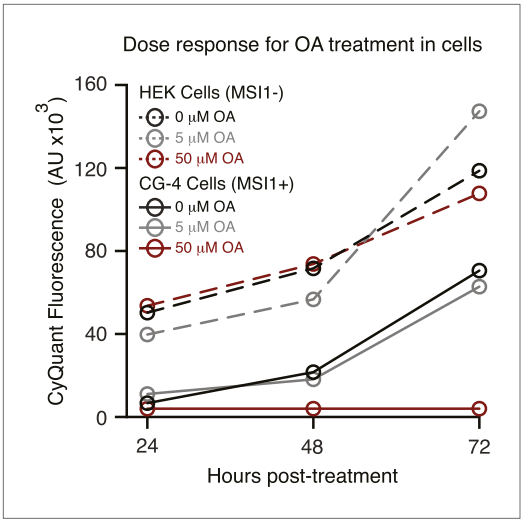

Figure 5—figure supplement 1. Dose response for oleic acid treatment in cell culture.
DOI: 10.7554/eLife.02848.016

A

Name	Mouse Scd1 3′ UTR fragment	Sequence	FP $K_{d, app}$ (nM)	F-EMSA $K_{d, app}$ (nM)
CCCR008	1	GGCAAAUAGUUGACC	79 ± 7	141 ± 8
CCCR006	2	CCCCAGAGAUUAGUGAGAUU	35 ± 9	54 ± 10
CCCR009	3	GGCAGGUAGUGGUAC	71 ± 4	66 ± 4
CCCR012	4	UGGGUGUAGUCUCUG	80 ± 7	157 ± 10
CCCR011	5	GGGAAUAGUCAAGA	380 ± 10	250 ± 20
CCCR010	6	AAUCUGUAGUGCCUG	85 ± 8	94 ± 7
CCCR013	7	CCAUCGUUUAGUCUACA	36 ± 11	36 ± 7

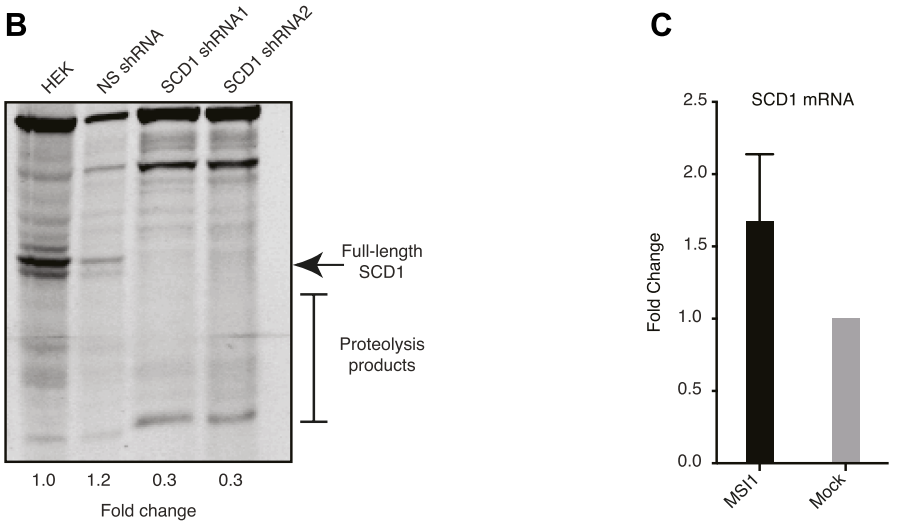

Figure 5—figure supplement 2.
DOI: 10.7554/eLife.02848.017

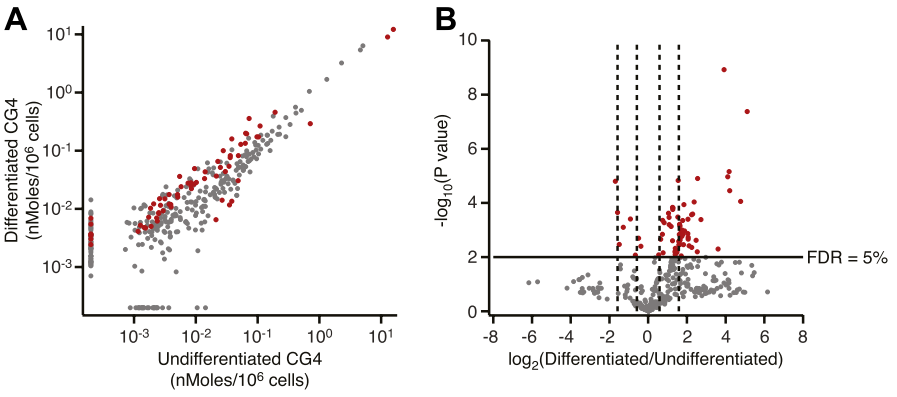

Figure 5—figure supplement 3. Lipidomics analysis of undifferentiated and differentiated CG4 oligodendrocyte progenitor cells.
DOI: 10.7554/eLife.02848.018

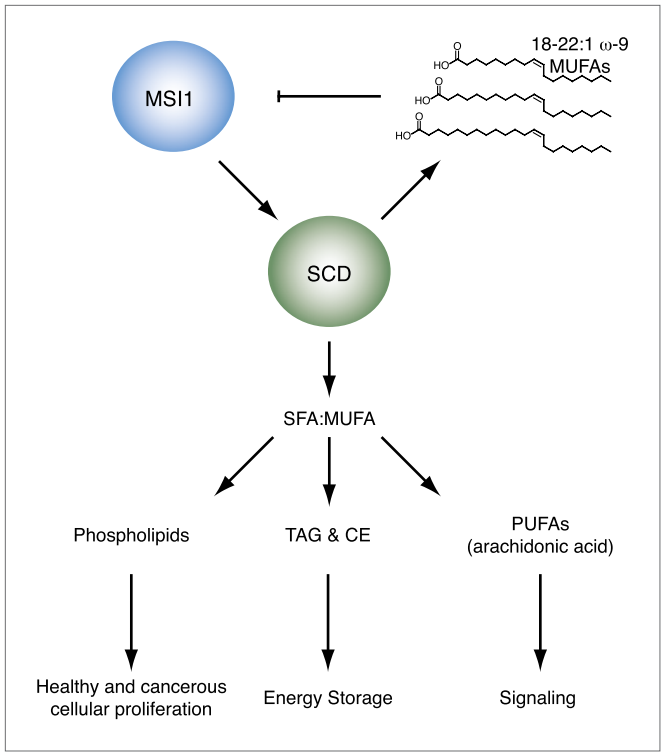

Figure 6. Model of SCD regulation by MSI1, and subsequent downstream consequences of SCD activity changes.
DOI: 10.7554/eLife.02848.019